Separation Science and Technology
Publication details, including instructions for authors and subscription information:
http://www.informaworld.com/smpp/title~content=t713708471

Non-Newtonian Flow for Retention Control in Field-Flow Fractionation

Josef Janča[ab]; J. Calvin Giddings[a]
[a] DEPARTMENT OF CHEMISTRY, UNIVERSITY OF UTAH SALT LAKE CITY, UTAH [b] Institute of Analytical Chemistry, Czechoslovak Academy of Sciences, Brno, Czechoslovakia

To cite this Article Janča, Josef and Giddings, J. Calvin(1981) 'Non-Newtonian Flow for Retention Control in Field-Flow Fractionation', Separation Science and Technology, 16: 7, 805 — 815
To link to this Article: DOI: 10.1080/01496398108058129
URL: http://dx.doi.org/10.1080/01496398108058129

SEPARATION SCIENCE AND TECHNOLOGY, 16(7), pp. 805–815, 1981

Non-Newtonian Flow for Retention Control in Field-Flow Fractionation

JOSEF JANČA* and J. CALVIN GIDDINGS

DEPARTMENT OF CHEMISTRY
UNIVERSITY OF UTAH
SALT LAKE CITY, UTAH 84112

Abstract

Retention in field-flow fractionation (FFF) can be altered and controlled by the introduction of different kinds of velocity profiles in the FFF channel. Here we propose the use of non-Newtonian fluid flow to manipulate retention in FFF. The flexible, three parameter Ellis equation, describing non-Newtonian behavior, is used to derive the dependence of retention ratio R on the dimensionless mean solute layer thickness λ. Numerical calculations show the way in which changes in the parameters of the Ellis equation change the velocity profile in the channel and therefore the shape of the R versus λ functions.

INTRODUCTION

Relative retention and separation in field-flow fractionation (FFF) can be controlled by varying the nature and strength of the applied field, or by controlling the flow profile in the FFF channel. Of the two choices, the applied field can be manipulated more conveniently. The utilization of wide ranging field conditions has therefore served as a major basis for developing FFF systems (*1–4*). However, greater versatility is expected if field variations can be combined with flow profile control. An initial step in this direction was recently developed in which thermogravitational flow was superimposed in various proportions on normal forced flow to yield a wide range of flow profiles (5). In this article we present a second approach in which flow profile control is to be gained by the utilization of non-Newtonian carrier fluids.

The separation of solute molecules or particles in a field-flow fractionation channel is due to the simultaneous influence or coupling of the different

*Present address: Institute of Analytical Chemistry, Czechoslovak Academy of Sciences, 611 42 Brno, Czechoslovakia.

velocity vectors in the carrier stream in the channel and the external field acting over the width of the channel (*6*). The external field induces a migration of solute molecules across the channel at mean velocity U. Molecular diffusion, characterized by diffusion coefficient D, works against the field-induced motion as solute piles up and forms a steep concentration gradient against the far channel wall. On reaching steady-state conditions, each different solute species is concentrated in a layer characterized by the mean thickness l, in which (*7*)

$$l = D/U \tag{1}$$

The value of l is different for each molecular species, depending on the ratio of the diffusion coefficient D to the field-induced mean velocity of migration U, the latter being proportional to the field strength. The distribution of molecular species across the channel depends on l according to the exponential equation (*8*)

$$c(x) = c_0 \exp(-x/l) \tag{2}$$

where $c(x)$ is the concentration of the solute at distance x from the wall where accumulation takes place, and c_0 is the concentration of the solute at that wall. The external field, which induces the migration of solute toward the wall, can be of various types including thermal (*9*, *10*), electrical (*11*), sedimentation (*12*), flow (*13*), and concentration (*14*). The present analysis is intended to be applicable to all of these external fields.

Different solute species are swept along by the flow at different average velocities by virtue of their unequal distribution over the velocity profile. The averaging of solute velocity over the profile is carried out by the general equation (*15*)

$$R = \frac{<c(x) \cdot v(x)>}{<c(x)> \cdot <v(x)>} \tag{3}$$

where R is the retention ratio, $v(x)$ is the velocity of the solvent streamline at a distance x from the accumulation wall, and $<c(x)>$ and $<v(x)>$ are, respectively, the mean values of solute concentration and velocity over the channel cross section.

Equation (3) can be used to demonstrate that retention is controlled by the strength of the applied field. The field strength determines solute drift velocity U and, consequently, l and $c(x)$ by virtue of Eqs. (1) and (2). Equation (3) shows, even more directly, that retention can be altered by changes in the flow profile $v(x)$. For normal parabolic flow, Eq. (3) then provides the well-known retention equation (*15*)

$$R = 6\lambda[\coth(1/2\lambda) - 2\lambda] \tag{4}$$

where λ is the dimensionless ratio l/w, w being the thickness of the FFF channel.

A disturbance of the parabolic velocity profile can be a secondary result of the applied field, as in the case of thermal FFF, where the temperature gradient across the channel produces a viscosity gradient and thus disturbs the parabolic flow. A different example is provided by thermogravitational FFF where the velocity profile is altered by convection in the channel (5).

Departures from the parabolic velocity profile may be used to control retention, given appropriate experimental conditions (5). Some theoretical relationships dealing with retention and peak broadening when the velocity profile is not parabolic and not symmetric have been given recently (*16*). A general polynomial was used to describe the nonparabolic velocity profile in the channel. The polynomial form may be used for most velocity profiles not symmetric with respect to the central plane of the channel and, in addition, can also be used for the symmetric parabolic velocity profile.

In this paper we evaluate the possibility of using non-Newtonian liquids to alter the velocity profile in FFF. In such a system, one could, if needed, program the parameters of the non-Newtonian carrier to change the shape of the velocity profile during an FFF separation.

THEORY

Most simple fluids flowing at moderate rates obey Newton's law in which the velocity gradient $dv(x)/dx$ is proportional to the shear stress τ_x:

$$\tau_x = \eta \frac{dv(x)}{dx} \tag{5}$$

The viscosity η is independent of shear stress for such Newtonian fluids. For non-Newtonian liquids, viscosity varies with the shear stress. The change in η with τ_x over the channel cross section alters the shape of the velocity profile in the channel, and parabolic flow is no longer realized.

Among various models describing velocity profiles for non-Newtonian flow, the Ostwald–de-Waele power law and the Ellis model (*17*) are the most convenient for practical calculations because the necessary parameters are available for many non-Newtonian liquids. The Ellis equation

$$\frac{dv(x)}{dx} = (\phi_0 + \phi_1 \mid \tau_x \mid^{\alpha-1})\tau_x \tag{6}$$

contains three adjustable parameters, ϕ_0, ϕ_1, and α. If $\alpha > 1$, the model yields results approaching Newton's law for small values of the shear stress

τ_x. Newton's law is also fulfilled when $\phi_1 = 0$ or $\alpha = 1$. When $\phi_0 = 0$, the Ellis equation reduces to the simple power law

$$\frac{dv(x)}{dx} = \phi_1 \mid \tau_x \mid^{\alpha-1} \tau_x \tag{7}$$

The flexibility of the Ellis equation is demonstrated by its easy conversion to Newtonian flow and the commonly used power law of Eq. (7). For this reason we use the Ellis equation for our theoretical development.

The shear stress τ_x in a parallel plate channel is given simply by

$$\tau_x = \frac{\Delta P}{L}\left(\frac{w}{2} - x\right) \tag{8}$$

where ΔP is the pressure drop along the length of the channel. For simplicity we define the pressure drop over a unit length of the channel by

$$\pi = \Delta P/L \tag{9}$$

and a new dimensionless coordinate by

$$\rho = x/w \tag{10}$$

Substituting Eqs. (9) and (10) into (8), we find

$$\tau_x = \pi w(\tfrac{1}{2} - \rho) \tag{11}$$

When this is substituted into Eq. (6) and integrated, an expression can be found for the velocity profile $v(x)$. For this purpose we use the boundary conditions $v(x) = 0$ for $\rho = 0$ and 1. Integration then yields

$$v(\rho) = \frac{\phi_0 \pi w^2}{8}[1 - (1 - 2\rho)^2] + \frac{\phi_1 \pi^\alpha}{\alpha + 1}\left(\frac{w}{2}\right)^{\alpha+1}[1 - \mid 1 - 2\rho \mid^{\alpha+1}] \tag{12}$$

The mean value of this velocity across the channel may be calculated from

$$<v(\rho)> = \int_0^1 v(\rho)\, d\rho \Big/ \int_0^1 d\rho \tag{13}$$

Substituting Eq. (12) into Eq. (13), integrating, and rearranging, we obtain

$$<v(\rho)> = \frac{\phi_0 \pi w^2}{12} + \frac{\phi_1 \pi^\alpha}{\alpha + 2}\left(\frac{w}{2}\right)^{\alpha+1} \tag{14}$$

When we express the concentration distribution in the channel in terms of the new coordinate system $\rho = x/w$, Eq. (2) assumes the form

$$c(\rho) = c_0 \exp(-\rho/\lambda) \tag{15}$$

where c_0 is concentration at the accumulation wall of the channel, $\rho = 0$. The mean concentration across the channel can be calculated from

$$<c(\rho)> = \frac{c_0 \int_0^1 \exp(-\rho/\lambda)\, d\rho}{\int_1^0 d\rho} \tag{16}$$

Integration and rearrangement of Eq. (16) give

$$<c(\rho)> = c_0\lambda[1 - \exp(-1/\lambda)] \tag{17}$$

The desired equation for retention ratio R is obtained by substitution of Eqs. (12), (14), (15), and (17) into Eq. (3), followed by integration. We have

$$R = \frac{2\phi_0\lambda[\exp(-1/\lambda)(1+2\lambda)+1-2\lambda]+2\phi_1\alpha!\lambda(\pi w/2)^{\alpha-1}[-\exp(1/\lambda)A_n - B_n - C]}{[1-\exp(-1/\lambda)]\left[\frac{\phi_0}{3} + \frac{\phi_1}{\alpha+2}\left(\frac{\pi w}{2}\right)^{\alpha-1}\right]} \tag{18}$$

where A_n, B_n, and C can be expressed as follows when α is an integer:

$$A_n = \sum_{n=1}^{\alpha+1} \frac{(2\lambda)^{n-1}}{(\alpha + 1 - n)!} \tag{19}$$

$$B_n = \sum_{n=1}^{\alpha+1} (-1)^n \frac{(2\lambda)^{n-1}}{(\alpha + 1 - n)!} \tag{20}$$

and

$$C = \exp(-1/2\lambda)(2\lambda)^{\alpha}[1 + (-1)^{\alpha}] \tag{21}$$

We noted above that when $\phi_1 = 0$, the velocity profile becomes parabolic (Newtonian), in which case Eq. (18) reduces to Eq. (4). The velocity profile also becomes Newtonian when $\alpha = 1$, and R is given in this case also by Eq. (4).

A different facet of the R vs λ relationship concerns the limiting case when λ approaches zero. Equation (18) may be simplified to

$$R = \frac{2\phi_0\lambda + 2\phi_1\alpha!\lambda\left(\frac{\pi w}{2}\right)^{\alpha-1}}{\frac{\phi_0}{3} + \frac{\phi_1}{\alpha+2}\left(\frac{\pi w}{2}\right)^{\alpha-1}} \tag{22}$$

For Newtonian liquids, when $\phi_1 = 0$ (or $\alpha = 1$), Eq. (22) becomes simply

$$R = 6\lambda \tag{23}$$

which is the limiting case, as λ tends to zero, of Eq. (4). When a non-Newtonian liquid is described by the power law, Eq. (22) reduces to

$$R = 2\alpha!(\alpha + 2)\lambda \tag{24}$$

which reduces to Eq. (23) for $\alpha = 1$, as expected.

RESULTS AND DISCUSSION

Velocity profiles calculated from Eqs. (12) and (14) are shown in Fig. 1 as a plot of dimensionless coordinate ρ versus $v/\langle v\rangle$, where v and $\langle v\rangle$ are, respectively, the flow velocity at a particular value of ρ and the average velocity in the channel. The curves in Fig. 1 show the effect of changing the value of α with all other parameters held constant. The range shown for α ($1 \leq \alpha \leq 9$) covers the likely range of practical applications. In the case when $\alpha = 1$, we have Newtonian behavior.

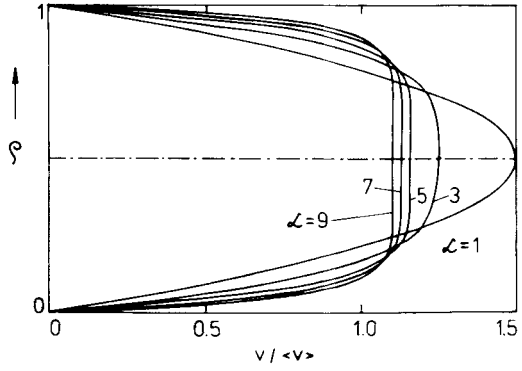

FIG. 1. Normalized velocity profiles for non-Newtonian flow in an FFF channel for different values of α. Input parameters are $\phi_0 = 0$ and $\phi_1 = 1$.

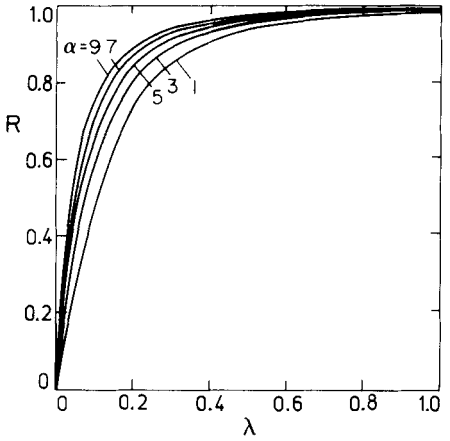

FIG. 2. Dependence of R on $\lambda(0 \leq \lambda \leq 1)$ for different values of α, calculated using Eq. (18). Input parameters are those for Fig. 1.

Figures 2 through 5 are all plots of retention ratio R versus the dimensionless layer thickness λ, and show the effects of varying different parameters in Eq. (18). Figure 2 shows the effect of changing α. Because $\phi_0 = 0$ for all cases, Eq. (6) reduces to the power law, Eq. (7), and α is the only factor influencing R vs λ. Values of α are in the same range as for Fig. 1, $1 \leq \alpha \leq 9$. We see from Fig. 2 that the R vs λ dependence is most pronounced when $0 \leq \lambda \leq 0.5$. This region is expanded in Fig. 3.

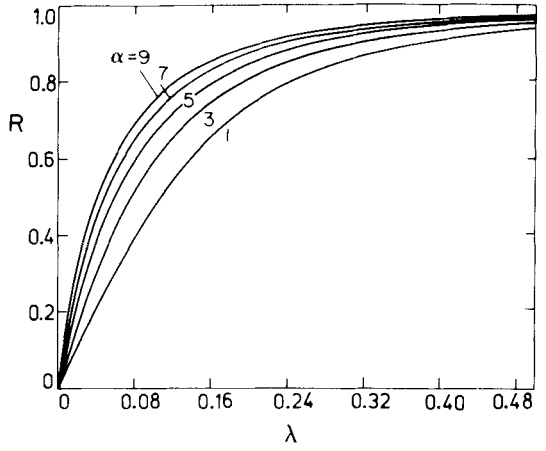

FIG. 3. Dependence of R on λ $(0 \leq \lambda \leq 0.5)$ for different values of α. This figure is an enlarged portion of Fig. 2 and has the same input parameters as Fig. 1.

Figures 2 and 3 show that R increases most steeply with λ for large α values. This can be explained in terms of the velocity profiles in Fig. 1. For large α values the velocity gradient is steep near the walls. A solute zone of a given thickness (λ value) therefore is swept along more rapidly the larger α, yielding a higher R value. In the limiting case of vanishingly small λ values, the initial slope of the R versus λ curve is shown by Eq. (24) to be $2\alpha!(\alpha + 2)$, which, of course, increases rapidly with α.

We must also consider the influence of the other parameters of Eq. (18) on R vs λ curves. The ratio of ϕ_0 to ϕ_1 plays an important role and describes the relative contributions of parabolic and nonparabolic velocity factors to the resultant profile. The effects of changing ϕ_0 and ϕ_1 with α held constant are shown in Figs. 4 ($\alpha = 3$) and 5 ($\alpha = 5$). The boundary curves, $\phi_0/\phi_1 = \infty$ and 0, correspond to the Newtonian parabolic velocity profile in the first case and to the power law in the second. Inside these bounding limits the curves vary continuously, demonstrating that by choosing conditions corresponding to different values for the ϕ_0/ϕ_1 ratio, we can continuously vary R vs λ functions. [We note that ϕ_0/ϕ_1 is not dimensionless but that $\phi_0/\phi_1(\pi w)^{\alpha-1}$

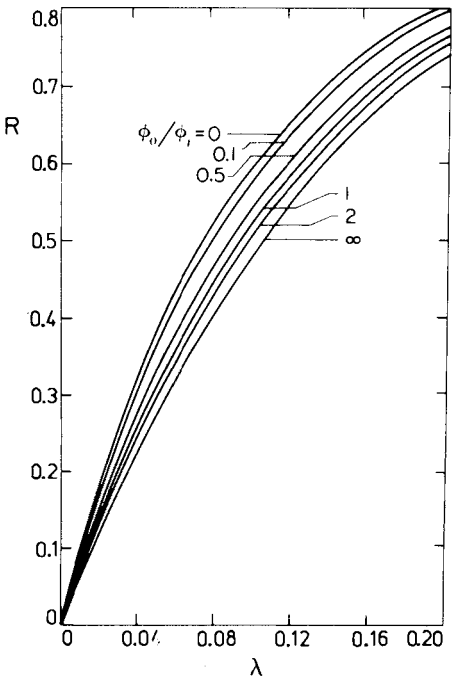

FIG. 4. Effect of different ϕ_0/ϕ_1 ratios on R vs λ functions, calculated using Eq. (18). Constant input parameters are $\alpha = 3$, $\pi = 2$, $w = 1$.

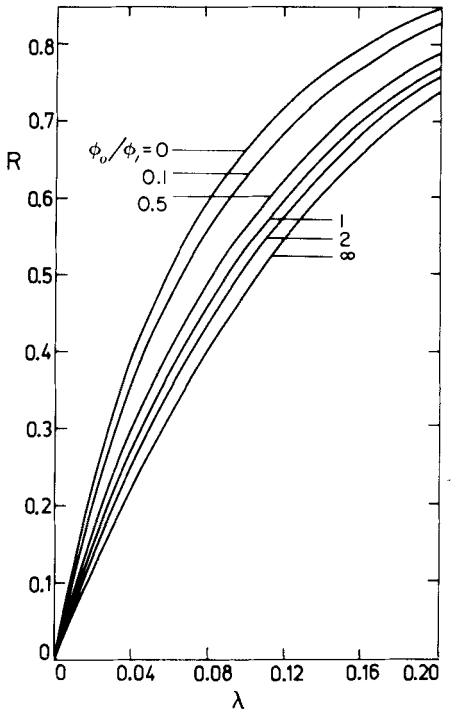

FIG. 5. Effect of different ϕ_0/ϕ_1 ratios on R vs λ functions. All parameters have identical values to those of Fig. 4 except $\alpha = 5$.

is. Since πw is held constant at 2 for the two plots, the above dimensionless group assumes values of $\phi_0/4\phi_1$ in Fig. 4 and $\phi_0/16\phi_1$ in Fig. 5.]

Lastly, to study the effect of changing π and w on the R vs λ functions, we note that in Eq. (18) these two parameters always appear together as the product πw. In view of the above dimensional arguments, Figs. 4 and 5 can be construed as reflecting changes in πw as much as in ϕ_0/ϕ_1, since, in reality, it is the dimensionless group $\phi_0/\phi_1(\pi w)^{\alpha-1}$ undergoing variation. Following this approach, the curves in Fig. 4 represent $\pi w = 2(\phi_0/\phi_1)^{1/2}/\gamma^{1/2}$, where γ is the "fixed" ϕ_0/ϕ_1 ratio shown in the figure; in Fig. 5 the corresponding expression is $\pi w = 2(\phi_0/\phi_1)^{1/4}/\gamma^{1/4}$. Thus Figs. 4 and 5 both show the trend, going left to right in each, of variations in πw from infinity to zero. As expected, as πw is reduced we get the same trend as when ϕ_0/ϕ_1 increases. Both trends represent a tendency toward normal parabolic flow.

Steric FFF (*18*) provides a special and possibly important case of the use of non-Newtonian behavior. In steric FFF, particles accumulate at the wall

or at a fixed distance from the wall, in place of the exponential distribution across the width of the channel represented for normal FFF systems by Eq. (2). A first approximation in the steric case gives

$$R = \frac{v(a/w)}{\langle v(\rho) \rangle} \tag{25}$$

where a is the particle radius. Using $\lambda_a = a/w$ and substituting Eqs. (12) and (14) into Eq. (25) yields

$$R = \frac{2\lambda_a(1 - \lambda_a)\phi_0 + \dfrac{\phi_1}{\alpha + 1}(\pi w/2)^{\alpha-1}[1 - |1 - 2\lambda_a|^{\alpha+1}]}{\dfrac{\phi_0}{3} + \dfrac{\phi_1}{\alpha + 2}(\pi w/2)^{\alpha-1}} \tag{26}$$

which for the Newtonian fluid ($\phi_1 = 0$) is reduced to the recognized expression (*8*)

$$R = 6\lambda(1 - \lambda) \tag{27}$$

which is an approximation of Eq. (4).

In this paper we have not attempted the detailed "engineering" of non-Newtonian FFF systems. This would involve attempting to find liquid carriers with appropriate non-Newtonian parameters. The non-Newtonian properties of certain one-phase systems may be changed radically by varying the concentration, or molecular weight, or nature of the dissolved polymer or biopolymer species (*19*). Other possibilities are the use of two-phase or multiphase systems such as suspensions, or mixtures of two or more immiscible liquids as carriers. Experimental complications such as the stabilization of these systems must, of course, be solved. However, it might be difficult to reach an adequate level of non-Newtonian behavior at the low flow velocities needed for high resolution FFF separations. Steric FFF might provide an interesting application in that case because higher flow velocities can be used, although not without causing serious departures from Eqs. (25) through (27).

The approach discussed above involves an intentional, controlled exploitation of the properties of non-Newtonian carrier fluids in FFF. A local and less controllable aspect, which should be taken into account in normal FFF separations using Newtonian carrier fluids, is the possible non-Newtonian behavior of the solute material being separated. (Local viscosity changes due to solute might be important even in the absence of non-Newtonian

behavior.) This may be anticipated in cases when high molecular weight species are separated. Factors such as concentration, molecular weight, and the shape and the flexibility of the separated species will affect the occurrence of non-Newtonian flow. These situations will complicate the shape of the velocity profile in the solute zone and thus disturb normal retention patterns. More work is needed to elucidate this phenomenon.

Acknowledgment

This research was supported by National Science Foundation Grant No. CHE 79–19879.

REFERENCES

1. F. J. F. Yang, M. N. Myers, and J. C. Giddings, *Anal. Chem., 46,* 1924 (1974).
2. F. J. F. Yang, M. N. Myers, and J. C. Giddings, *J. Colloid Interfac. Sci., 60,* 574 (1977).
3. J. C. Giddings, S. R. Fisher, and M. N. Myers, *Am. Lab., 10,* 15 (1978).
4. J. C. Giddings, K. D. Caldwell, J. F. Moellmer, T. H. Dickinson, M. N. Myers, and M. Martin, *Anal. Chem., 51,* 30 (1979).
5. J. C. Giddings, M. Martin, and M. N. Myers, *Sep. Sci. Technol., 14,* 611 (1979).
6. J. C. Giddings, *Sep. Sci., 1,* 123 (1966).
7. E. Grushka, K. D. Caldwell, M. N. Myers, and J. C. Giddings, *Sep. Purif. Methods, 2,* 127 (1973).
8. J. C. Giddings, *J. Chem. Educ., 50,* 667 (1973).
9. G. H. Thompson, M. N. Myers, and J. C. Giddings, *Sep. Sci., 2,* 797 (1967).
10. G. H. Thompson, M. N. Myers, and J. C. Giddings, *Anal. Chem., 41,* 1219 (1969).
11. K. D. Caldwell, L. F. Kesner, M. N. Myers, and J. C. Giddings, *Science, 176,* 296 (1972).
12. J. C. Giddings, F. J. F. Yang, and M. N. Myers, *Anal. Chem., 46,* 1917 (1974).
13. J. C. Giddings, F. J. F. Yang, and M. N. Myers, *Science, 193,* 1244 (1976).
14. J. C. Giddings, F. J. F. Yang, and M. N. Myers, *Sep. Sci., 12,* 381 (1977).
15. M. E. Hovingh, G. H. Thompson, and J. C. Giddings, *Anal. Chem., 42,* 195 (1970).
16. M. Martin and J. C. Giddings, *J. Phys. Chem.*, Accepted.
17. R. B. Bird, W. E. Stewart, and E. N. Lightfoot, *Transport Phenomena*, Wiley, New York, 1960.
18. J. C. Giddings and M. N. Myers, *Sep. Sci. Technol., 13,* 637 (1978).
19. T. G. Fox, Jr., J. C. Fox, and P. J. Flory, *J. Am. Chem. Soc., 73,* 1901 (1951).

Received by editor June 12, 1980